

FREQCa: ACCELERATING DIFFUSION MODELS VIA FREQUENCY-AWARE CACHING

Jiacheng Liu^{1,2,3*} Peiliang Cai^{1*} Qinming Zhou^{1,4} Yuqi Lin^{1,5} Deyang Kong^{1,7}

Benhao Huang^{1,6} Yupei Pan^{1,7} Haowen Xu¹ Chang Zou^{1,2,7} Junshu Tang²

Shikang Zheng^{1,8} Linfeng Zhang^{1†}

¹EPIC Lab,STJU ²Tencent Hunyuan ³SDU ⁴THU ⁵JLU ⁶CMU ⁷UESTC ⁸SCUT

ABSTRACT

The application of diffusion transformers is suffering from their significant inference costs. Recently, feature caching has been proposed to solve this problem by reusing features from previous timesteps, thereby skipping computation in future timesteps. However, previous feature caching assumes that features in adjacent timesteps are similar or continuous, which does not always hold in all settings. To investigate this, this paper begins with an analysis from the frequency domain, which reveal that *different frequency bands in the features of diffusion models exhibit different dynamics across timesteps*. Concretely, low-frequency components, which decide the structure of images, exhibit higher *similarity* but poor continuity. In contrast, the high-frequency bands, which decode the details of images, show significant continuity but poor similarity. These interesting observations motivate us to propose **Frequency-aware Caching (FreqCa)** which directly reuses features of low-frequency components based on their similarity, while using a second-order Hermite interpolator to predict the volatile high-frequency ones based on its continuity. Besides, we further propose to cache Cumulative Residual Feature (CRF) instead of the features in all the layers, which reduces the memory footprint of feature caching by **99%**. Extensive experiments on FLUX.1-dev, FLUX.1-Kontext-dev, Qwen-Image, and Qwen-Image-Edit demonstrate its effectiveness in both generation and editing. *Codes are available in the supplementary materials and will be released on GitHub.*

1 INTRODUCTION



Figure 1: Images sampled by Qwen-image with *FreqCa* with $7.14\times$ acceleration.

*Equal contribution.

†Corresponding author. Email: zhanglinfeng@sjtu.edu.cn

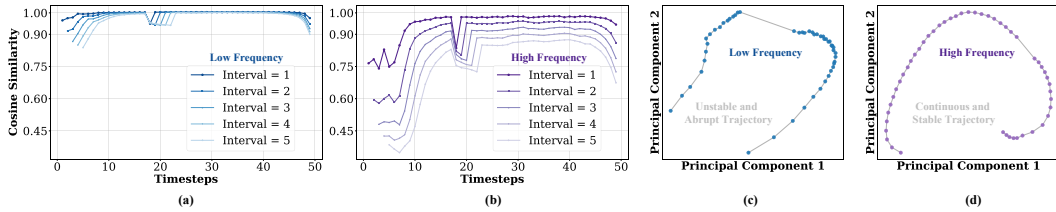


Figure 2: **Analysis from the frequency perspective.** (a)-(b): Temporal similarity analysis using cosine similarity for low-frequency and high-frequency components across different step intervals. (c)-(d): Feature trajectory visualized via Principal Component Analysis (PCA).

Diffusion Models (DMs) have achieved remarkable success in generative tasks like image synthesis and video generation (Ho et al., 2020a; Rombach et al., 2022; Blattmann et al., 2023). The recent introduction of Diffusion Transformers (Peebles & Xie, 2023a) has further advanced generation quality and diversity, establishing them as the predominant architecture for large-scale visual content creation. However, diffusion transformers typically rely on a stack of heavy transformer blocks and multi-step sampling, making computational efficiency a critical bottleneck for their practical deployment. To address this, the paradigm of feature caching has emerged, which exploits the high temporal redundancy between adjacent timesteps for acceleration (Ma et al., 2024; Li et al., 2023a; Selvaraju et al., 2024; Chen et al., 2024; Zou et al., 2025; 2024).

The debate of caching paradigms. Feature caching has gradually emerged into two different paradigms. The paradigm of “Cache-Then-Reuse” assumes that the features of DM in adjacent timesteps are highly **similar** and thus proposes to directly **reuse** the features of previous timesteps in the future timesteps (Selvaraju et al., 2024). In contrast, the paradigm of “Cache-Then-Forecast” assumes that features of DM are “continuous” and thus proposes to forecast features in the future timesteps based on features in the previous timesteps with non-parametric predictors such as Taylor expansion. Although the paradigm “Cache-Then-Forecast” tends to show better performance in recent works, their assumption of continuity does not always hold perfectly. For instance, Liu *et al.* demonstrates that features of FLUX are not high-order continuous, making TaylorSeer degenerate into a linear prediction method and thus suffer from quality loss (Liu et al., 2025a). Based on these findings, this paper begins with an in-depth analysis of the temporal dynamics of diffusion models.

Analysis from the frequency perspective. In classical image processing, the high-frequency and low-frequency components of images are usually considered as carrying different semantic information, which motivates us to study the dynamics of high-frequency and low-frequency components in the feature of diffusion models separately. As shown in Figure 2(a)-(b), surprisingly, we find different frequency exhibits significantly different dynamics. Concretely, the similarity of low-frequency is higher than 0.90 at most timesteps, while the high-frequency exhibits clearly low similarity. On the other hand, as shown in Figure 2(c)-(d), the feature trajectory of high-frequency shows perfect stability and continuity, while the feature trajectory of low-frequency is unstable and accompanied by sudden mutation, indicating that the high-frequency information can be accurately predicted while the low-frequency information fails.

Based on the above observations, this paper introduces **Frequency-aware Feature Caching (FreqCa)**, which aims to decouple the frequency of the features in diffusion models and treat them in different paradigms. Concretely, *FreqCa* applies any frequency decomposition (*e.g.*, *Fourier Transformation*) to the cached features. For the low-frequency bands, we directly reuse them in the future timesteps because of their *high similarity*. For the high-frequency bands, we predict their values in the future timesteps with any sequential predictor (*Hermite polynomial predictor*) for their *good continuity*. Then, in the future timesteps, *FreqCa* reconstructs the features based on the reused low-frequency bands and predicted high-frequency bands, enabling it to skip the computation over diffusion transformers, achieving the best cooperation between the previous caching paradigms.

Memory-Efficient Feature Caching. The previous caching methods usually cache all the features from attention and FFN layers, leading to significant memory costs (*e.g.*, $\geq 10G$ memory costs on FLUX in ToCa), preventing feature caching methods from real-world applications. As discussed by Veit et al. (2016), neural networks with residual connections can be considered as an ensemble of features in all blocks, which motivates us to propose caching the Cumulative Residual Feature (CRF), *i.e.*, the cumulative features of all the residual connections from attention and FFN blocks. This trick helps us reduce the memory footprint from caching $2 \times L$ (L indicates layer counts) features into

a single feature vector, slashing cache memory usage by up to 99%. Besides, it also reduces the number of frequency (reverse) decomposition operations by $2L$ times, making them account for only $\leq 0.01\%$ latency costs during the whole diffusion process.

In summary, this contribution of this paper is as follows.

- **Frequency-Aware Feature Caching:** Motivated by the difference in similarity and continuity of different frequency bands, we propose *FreqCa*, which applies different feature caching methods to different frequencies, unifying the two previous caching paradigms.
- **Memory-Efficient Feature Caching** By caching only the Cumulative Residual Feature, *FreqCa* achieves $\mathcal{O}(1)$ memory complexity, slashing Cache memory usage to a mere **1%** of prior approaches without fidelity loss, enabling high-quality acceleration on consumer hardware.
- **State-of-the-art generalization and performance:** Across text-to-image generation and image editing tasks, *FreqCa* consistently delivers $6\text{--}7\times$ acceleration with quality degradation below 2%, outperforming existing methods and demonstrating strong robustness and practicality.

2 RELATED WORKS

Diffusion models have emerged as a cornerstone of modern generative AI, exhibiting state-of-the-art capabilities in synthesizing visual content (Sohl-Dickstein et al., 2015; Ho et al., 2020b). While early models were predominantly built upon U-Net architectures (Ronneberger et al., 2015), their scalability limitations paved the way for the Diffusion Transformer (DiT) (Peebles & Xie, 2023b). The DiT architecture has since become foundational, catalyzing a wave of powerful models across diverse domains (Zheng et al., 2024; Yang et al., 2025). Nevertheless, the iterative nature of the diffusion sampling process imposes a significant computational burden during inference, making acceleration a critical area of research (Ho et al., 2020b; Peebles & Xie, 2023b). Current efforts to enhance efficiency are largely focused on two complementary directions: reducing the number of sampling steps and accelerating the denoising network itself.

2.1 SAMPLING Timestep Reduction

One primary strategy seeks to minimize the number of required sampling iterations while preserving generation quality. Seminal work like DDIM introduced deterministic sampling to reduce step counts without significant fidelity loss (Song et al., 2021). This concept was further refined by the DPM-Solver series, which employed high-order ODE solvers to achieve faster convergence (Lu et al., 2022a;b; Zheng et al., 2023). Other notable approaches include knowledge distillation, which trains a student model to emulate multiple denoising steps of a larger teacher model (Salimans & Ho, 2022; Meng et al., 2022), and Rectified Flow, which learns to straighten the generation path between noise and data distributions (Liu et al., 2023b). More recently, Consistency Models have enabled high-quality synthesis in a single step by directly mapping noise to clean data, circumventing the need for a sequential path (Song et al., 2023).

2.2 DENOISING NETWORK ACCELERATION

An alternative to reducing timesteps is to decrease the computational cost of each forward pass through the denoising network. This is typically achieved via model compression or feature caching.

Model Compression-based Acceleration. One avenue involves model compression, which includes techniques such as network pruning (Fang et al., 2023; Zhu et al., 2024), quantization (Li et al., 2023b; Shang et al., 2023; Kim et al., 2025), and various forms of token reduction that dynamically shorten the input sequence length (Bolya & Hoffman, 2023; Kim et al., 2024; Zhang et al., 2024; 2025). While effective, these methods often necessitate a fine-tuning or retraining stage to mitigate the potential loss of expressive power inherent in model simplification (Li et al., 2024; 2023b).

Feature Caching-based Acceleration. A compelling training-free alternative is feature caching, which exploits temporal redundancies in the denoising process. Pioneered in U-Net architectures through FasterDiffusion and DeepCache, this paradigm was subsequently adapted to DiTs. Initial efforts focused on a “cache then reuse” strategy, while advanced techniques like FORA and Δ -DiT refined this approach. This concept evolved with more sophisticated mechanisms, including dynamic token-level updates (ToCa), adaptive sampling (RAS (Liu et al., 2025c)), and explicit error correction frameworks (Qiu et al., 2025; Chen et al., 2025; Chu et al., 2025). A pivotal shift was the “cache then forecast” paradigm introduced by TaylorSeeer, which was further advanced by more robust numerical methods in FoCa (Zheng et al., 2025), HiCache (Feng et al., 2025), and SpeCa (Liu et al., 2025b).

However, a crucial flaw underlies these sophisticated paradigms, as hinted at by preliminary frequency-domain analyses. For instance, PAB (Zhao et al., 2024) insightfully associated different attention mechanisms with distinct frequency bands but did not delve into token-level frequency dynamics. Similarly, while FasterCache (Lv et al., 2025) examined the frequency-domain differences within Classifier-Free Guidance, its findings were confined to this specific context, not addressing the more universal dynamics of temporal feature evolution and thus showing limited practical acceleration.

In contrast to prior methods that treat features as a monolithic whole, we propose **FreqCa**, which resolves quality degradation in caching by decomposing features into their stable low-frequency and volatile high-frequency components for differentiated treatment. As an added benefit, we introduce the Cumulative Residual Feature, collapsing the memory complexity from $\mathcal{O}(L)$ to $\mathcal{O}(1)$ to solve the resource inefficiency of prior “layer-wise” architectures.

3 METHOD

3.1 PRELIMINARY

3.1.1 DIFFUSION TRANSFORMER ARCHITECTURE.

The Diffusion Transformer (DiT) (Peebles & Xie, 2023a) employs a hierarchical structure $\mathcal{G} = g_1 \circ g_2 \circ \dots \circ g_L$, where each module $g_l = \mathcal{F}_{\text{SA}}^l \circ \mathcal{F}_{\text{CA}}^l \circ \mathcal{F}_{\text{MLP}}^l$ is composed of self-attention (SA), cross-attention (CA), and multilayer perceptron (MLP) components. In DiT, these components are dynamically adapted over time to handle different noise levels during the image generation process. The input $\mathbf{x}_t = \{\mathbf{x}_i\}_{i=1}^{H \times W}$ is represented as a sequence of tokens corresponding to image patches. Each module integrates information through residual connections of the form $\mathcal{F}(\mathbf{x}) = \mathbf{x} + \text{AdaLN} \circ f(\mathbf{x})$, where AdaLN denotes adaptive layer normalization, which stabilizes training and improves learning effectiveness.

3.1.2 FREQUENCY DECOMPOSITION METHODS

Frequency decomposition, through methods like the Fast Fourier Transform (FFT) and Discrete Cosine Transform (DCT), is a powerful technique for decoupling signals into distinct components. This process separates a signal into its **low-frequency** components, which typically represent global structure and smooth layouts, and its **high-frequency** components, which correspond to fine-grained details and sharp edges. In the context of diffusion models, this decoupling allows us to differentiate between stable, foundational structures and volatile, transient details along the generative trajectory.

3.2 FREQUENCY-AWARE CACHE ACCELERATION FRAMEWORK

In this section, we introduce the **FreqCa (Frequency-aware Feature Caching)** framework, which is built upon three key components: (i) performing frequency decomposition on the feature to be cached and applying separate strategies for its low- and high-frequency components; (ii) employing a nonlinear Hermite-polynomial-based predictor for the high-frequency part to improve prediction accuracy; and (iii) identifying the Cumulative Residual Feature (CRF) as a novel, highly efficient single-tensor caching target that encapsulates the entire transformation history of the model.

1. Frequency-Decomposed Caching and Prediction Strategy. Our differentiated caching strategy is motivated by the distinct temporal dynamics of frequency components. Low-frequency components exhibit high similarity but low continuity, making them stable but difficult to predict. Conversely, high-frequency components are less similar but more continuous, making them volatile yet predictable along a trajectory. This key difference means that a one-size-fits-all approach is not the best and that a differentiated strategy is required.

To implement this, we first decompose the feature \mathbf{z}_t into its constituent parts using a generic frequency transform $\mathcal{D}(\cdot)$:

$$\mathbf{z}_t = \mathbf{z}_t^{\text{low}} + \mathbf{z}_t^{\text{high}}, \quad \text{where} \quad \mathbf{z}_t^{\text{low/high}} = \mathcal{P}_{\text{low/high}}(\mathcal{D}(\mathbf{z}_t)).$$

Here, $\mathcal{P}_{\text{low/high}}$ are complementary projection operators. The low-frequency part governs global structure, while the high-frequency part encodes fine details.

Based on their dynamics, we apply tailored strategies. For the **stable low-frequency component** $\mathbf{z}_t^{\text{low}}$, we apply a direct reuse strategy to maintain global consistency with negligible cost: $\hat{\mathbf{z}}_t^{\text{low}} = \mathbf{z}_{t-1}^{\text{low}}$.

For the **predictable high-frequency component** $\mathbf{z}_t^{\text{high}}$, we employ a nonlinear predictor based on Hermite polynomials to accurately forecast its trajectory. Each high-frequency coefficient \hat{h}_i at a

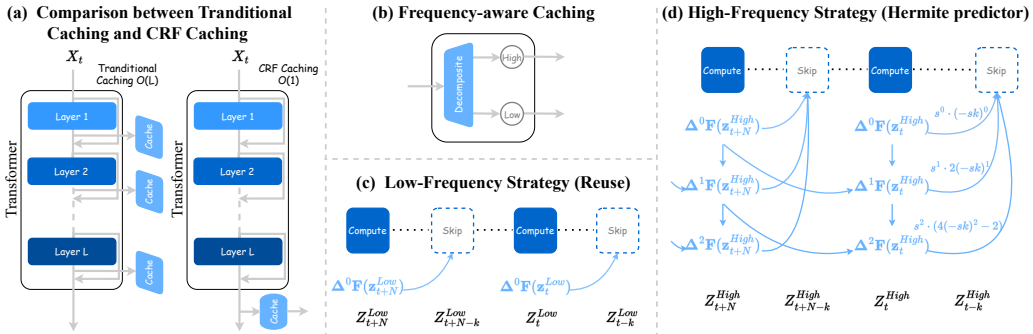


Figure 3: **Overview of the FreqCa framework.** (a) **CRF Caching**: Instead of caching features at every layer, we cache only the single Cumulative Residual Feature (CRF) at the end. (b) **Frequency-aware Caching**: The cached features are separated into low- and high-frequency bands using frequency decomposition techniques such as FFT or DCT. (c) **Low-Frequency Strategy (Reuse)**: Low-frequency component is directly reused from the prior step. (d) **High-Frequency Strategy (Hermite predictor)**: High-frequency component is forecasted using a Hermite predictor fitted on the last two activated steps.

normalized time $s_t \in [-1, 1]$ is modeled as: $\hat{h}_i(s_t) = \sum_{k=0}^m c_{i,k} \text{He}_k(s_t)$, where the coefficients $c_{i,k}$ are estimated via least-squares regression from the K most recent cached steps. This yields the precisely reconstructed high-frequency component \hat{z}_t^{high} .

Finally, the two components are recombined to yield the final predicted feature, $\hat{z}_t = \hat{z}_t^{\text{low}} + \hat{z}_t^{\text{high}}$.

2. Cumulative Residual Feature (CRF) At its core, a Diffusion Transformer (DiT) is a deep stack of L residual blocks. The transformation at each block l is not a replacement but an incremental update, as described by the standard residual connection: $\mathbf{h}^{(l+1)} = \mathbf{h}^{(l)} + \mathcal{F}^{(l)}(\mathbf{h}^{(l)}, t)$, where $\mathcal{F}^{(l)}(\cdot, t)$ denotes the transformation module at layer l (including Attention, and MLP), which is dynamically modulated by the diffusion timestep t (e.g., through AdaLN).

The structure of the DiT’s final output is thus revealed: $\phi_L(\mathbf{x}_t) = \mathbf{h}^{(0)} + \sum_{l=0}^{L-1} \mathcal{F}^{(l)}(\mathbf{h}^{(l)}, t)$. This formulation shows that the final output is not just another intermediate feature, but the **accumulation of the initial input and all subsequent residual updates**. We define this special output $\mathbf{z}_t \triangleq \phi_L(\mathbf{x}_t)$ and name it the **Cumulative Residual Feature (CRF)**, reflecting its composite nature.

This insight leads to a more memory-efficient strategy. While conventional layer-wise caching must store all intermediate features $\{\mathbf{h}^{(l)}\}_{l=0}^{L-1}$, our approach uses the fact that the CRF already contains the entire transformation history. We use this single, globally fused tensor as a highly efficient replacement for the full feature set. As shown in Figure 4, caching only the CRF achieves nearly identical reconstruction fidelity to full layer-wise caching, incurring only a 4% higher MSE on average, which confirms that the CRF acts as a near-lossless compression of the entire computational path. This makes it an ideal lightweight caching target, enabling a revolutionary reduction in memory complexity from $\mathcal{O}(L)$ to $\mathcal{O}(1)$ without a meaningful sacrifice in quality.

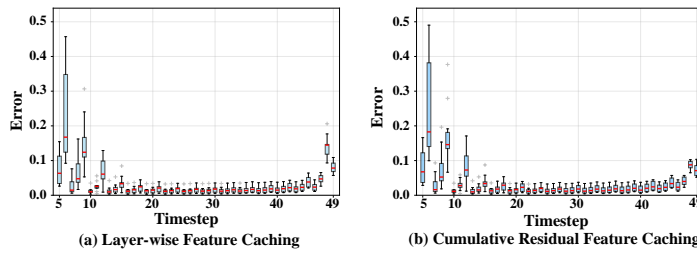


Figure 4: Box plots of Mean Squared Error (MSE) between ground-truth and predicted features per timestep. (a) layer-wise feature caching and (b) cumulative residual feature (CRF) caching.

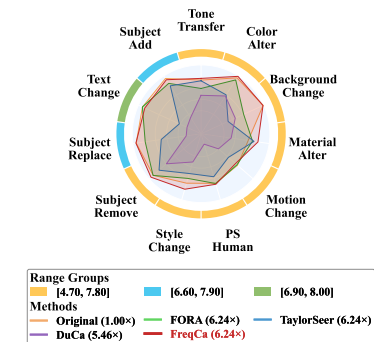


Figure 5: Gedit Benchmark on Qwen-Image-Edit, *FreqCa* outperforms most baselines.

4 EXPERIMENT

4.1 EXPERIMENT SETTINGS

Model Configurations. The experiments are conducted on four state-of-the-art visual generative models—**FLUX.1-dev** (Labs, 2024), **Qwen-Image** (Liu et al., 2023a), **FLUX.1-Kontext-dev** (Zhang & Agrawala, 2025), and **Qwen-Image-Edit** (Salimans & Ho, 2022).

Evaluation and Metrics. For the text-to-image generation evaluation, we adopt the DrawBench (Saharia et al., 2022) benchmark. The generated samples are systematically evaluated using ImageReward (Xu et al., 2023) and CLIP Score (Hessel et al., 2021), which jointly measure image quality and text-image semantic alignment. To assess visual fidelity, we further employ PSNR, SSIM (Wang et al., 2004) and LPIPS (Zhang et al., 2018), thereby capturing both pixel-level similarity and perceptual consistency. Additionally, we evaluate general-purpose image editing using the GEdit benchmark (Wang et al., 2024), which systematically assesses instruction-driven editing fidelity and alignment to target modifications under textual and visual guidance.

4.2 TEXT-TO-IMAGE GENERATION

4.2.1 FLUX.1-DEV

Table 1: **Quantitative comparison in text-to-image generation** for FLUX.1-dev and FLUX.1-schnell(a distilled version). Best results are highlighted in **bold**, and second-best are underlined.

Method	Acceleration				Quality Metrics		Perceptual Metrics		
	Latency(s) ↓	Speed ↑	FLOPs(T) ↓	Speed ↑	ImageReward↑	CLIP↑	PSNR↑	SSIM↑	LPIPS↓
[dev]: 50 steps	23.24 (+0.0%)	1.00×	3726.87	1.00×	0.99 (+0.0%)	32.64 (+0.0%)	∞	1.00	0.00
60% steps	14.12 (-39.2%)	1.65×	2236.12	1.67×	0.97 (-2.0%)	32.66 (+0.1%)	30.31	0.78	0.25
50% steps	11.82 (-49.1%)	1.97×	1863.44	2.00×	0.97 (+2.0%)	32.57 (-0.2%)	29.56	0.73	0.31
PAB	17.84 (-23.2%)	1.30×	3013.13	1.24×	0.95 (-4.0%)	32.55 (-0.3%)	28.84	0.67	0.40
DBCach e	16.88 (-27.4%)	1.38×	2384.29	1.56×	1.01 (+2.0%)	32.53 (-0.3%)	33.86	0.87	0.12
FORA ($N=3$)	9.06 (-61.0%)	2.57 ×	1267.89	2.94 ×	0.93 (-6.1%)	32.89 (+0.8%)	28.86	0.66	0.40
TeaCache ($l=0.6$)	9.13 (-60.7%)	2.55×	1342.20	2.78×	0.91 (-8.1%)	32.11 (-1.6%)	29.03	0.68	0.40
TaylorSeer ($N=3$, $O=2$)	10.16 (-56.3%)	2.29×	1416.92	2.63×	1.01 (+2.0%)	32.86 (+0.7%)	30.77	0.78	0.23
FreqCa ($N=3$)	9.37 (+50.7%)	2.48 ×	1417.40	2.63 ×	<u>1.00</u> (+1.0%)	32.61 (-0.1%)	33.03	0.86	0.13
FORA($N=5$) \dagger	5.97 (-74.3%)	3.89×	820.80	4.54×	0.82 (-17.2%)	32.48 (-0.5%)	28.44	0.60	0.50
ToCa($N=8$, $R=75\%$)	12.39 (-46.7%)	1.88×	829.86	4.49×	0.95 (-4.0%)	32.60 (-0.1%)	29.07	0.64	0.43
DuCa($N=8$, $R=70\%$)	9.40 (-59.6%)	2.47×	858.27	4.34×	0.94 (-5.1%)	32.58 (-0.2%)	29.06	0.64	0.43
TeaCache($l=1.0$) \dagger	7.07 (-69.6%)	3.29×	820.55	4.54×	0.84 (-15.2%)	31.88 (-2.3%)	28.61	0.64	0.48
TaylorSeer($N=6$, $O=2$)	6.73 (-71.0%)	3.45×	746.28	4.99 ×	<u>1.00</u> (+1.0%)	32.91 (+0.8%)	28.94	0.66	0.40
FreqCa ($N=7$)	5.19 (+77.7%)	4.48 ×	746.03	4.99 ×	1.01 (+2.0%)	32.98 (+1.0%)	30.00	0.71	0.31
FORA($N=7$) \dagger	5.09 (-78.1%)	4.57×	597.25	6.24 ×	0.68 (-31.3%)	31.90 (-2.3%)	28.32	0.59	0.54
ToCa($N=12$, $R=85\%$) \dagger	9.82 (-57.7%)	2.37×	618.57	6.02×	0.80 (-19.2%)	32.32 (-1.0%)	28.70	0.60	0.52
DuCa($N=12$, $R=80\%$) \dagger	7.74 (-66.7%)	3.00×	646.97	5.76×	0.77 (-22.2%)	32.20 (-1.3%)	28.71	0.60	0.53
TeaCache($l=1.4$) \dagger	6.14 (-73.6%)	3.79×	671.51	5.55×	0.74 (-25.3%)	31.78 (-2.6%)	28.12	0.48	0.68
TaylorSeer($N=9$, $O=2$) \dagger	5.85 (-74.8%)	3.97×	597.25	6.24 ×	0.86 (-13.1%)	32.04 (-1.8%)	28.38	0.59	0.51
FreqCa ($N=10$)	4.25 (+81.7%)	5.47 ×	597.47	6.24 ×	0.97 (+2.0%)	32.53 (-0.3%)	28.77	0.62	0.43
[schnell]: 4 steps	2.17 (+0.0%)	1.00×	278.41	1.00×	0.93 (+0.0%)	34.09 (+0.0%)	∞	1.00	0.00
FreqCa ($N=3$): 4 steps	1.29 (+40.6%)	1.68×	139.23	2.00×	0.95 (+2.2%)	34.47 (+1.1%)	30.30	0.81	0.16

• \dagger Methods exhibit significant degradation in image quality.

• Gray: Baseline-relative degradation in quality and gains in latency. Blue: **FreqCa** achieves minimal degradation with large latency gains.

On FLUX.1-dev, *FreqCa* consistently outperforms state-of-the-art acceleration methods across different speedup levels. At **2.63**× speedup, *FreqCa* achieves an **ImageReward of 1.00**, clearly outperforming FORA and TeaCache. At **4.99**× speedup, it maintains lossless quality. Even under **6.24**× speedup, *FreqCa* achieves only a **2%** drop in ImageReward (0.97), while TaylorSeer suffers a degradation of **13.1%**. *FreqCa* also achieves **2.00**× speedup on distilled FLUX.1-schnell while improving ImageReward from 0.93 to 0.95.

4.2.2 QWEN-IMAGE

On Qwen-Image, *FreqCa* demonstrates superior performance across different acceleration levels. At **5.00**× speedup, *FreqCa* achieves an ImageReward of **1.20**, outperforming TaylorSeer (1.01). At **7.14**× speedup, *FreqCa* shows only a **18.4%** drop in ImageReward (1.02), while TaylorSeer suffers a **41.6%** quality loss (0.73). *FreqCa* achieves **4.00**× speedup on distilled Qwen-Image-Lightning with minimal quality degradation.

Table 2: **Quantitative comparison in text-to-image generation** for Qwen-Image and Qwen-Image-Lightning (a distilled version). Best results are highlighted in **bold**, and second-best are underlined.

Method	Acceleration				Quality Metrics		Perceptual Metrics		
	Latency(s) \downarrow	Speed \uparrow	FLOPs(T) \downarrow	Speed \uparrow	ImageReward \uparrow	CLIP \uparrow	PSNR \uparrow	SSIM \uparrow	LPIPS \downarrow
50 steps	127.40 (+0.0%)	1.00 \times	12917.56	1.00 \times	1.25 (+0.0%)	35.59 (+0.0%)	∞	1.00	0.00
50% steps	64.10 (-49.6%)	1.99 \times	6458.78	2.00 \times	1.20 (-4.0%)	35.31 (-0.6%)	30.54	0.75	0.28
20% steps \dagger	25.92 (-79.6%)	4.89 \times	2583.51	5.00 \times	0.94 (-26.4%)	34.95 (-1.0%)	28.59	0.61	0.52
FORA($N=4$)\dagger	38.43 (-70.0%)	3.32 \times	3359.99	3.84 \times	0.93 (-25.6%)	34.40 (-3.3%)	28.66	0.59	0.51
ToCa($N=8, R=75\%$)\dagger	61.37 (-51.8%)	2.08 \times	2991.34	4.32 \times	1.02 (-18.4%)	34.96 (-1.8%)	28.93	0.63	0.44
DuCa($N=9, R=80\%$)\dagger	34.73 (-72.7%)	3.67 \times	2958.13	4.37 \times	0.77 (-38.4%)	34.62 (-2.7%)	28.45	0.58	0.55
TaylorSeer($N=6$)	<u>30.75</u> (-75.9%)	<u>4.14</u> \times	2583.97	5.00 \times	1.01 (-19.2%)	34.71 (-2.5%)	28.58	0.62	0.46
FreqCa($N=6$)	29.80 (-76.6%)	4.28 \times	<u>2584.70</u>	<u>5.00</u> \times	1.20 (-4.0%)	35.39 (-0.6%)	29.67	0.78	0.33
FORA($N=6$)\dagger	28.69 (-77.5%)	4.44 \times	2326.74	5.55 \times	0.48 (-61.6%)	33.34 (-6.3%)	28.48	0.55	0.59
ToCa($N=12, R=85\%$)\dagger	50.95 (-60.0%)	2.50 \times	2406.20	5.37 \times	0.55 (-56.0%)	34.08 (-4.2%)	28.69	0.57	0.53
DuCa($N=12, R=90\%$)\dagger	28.57 (-77.6%)	4.46 \times	2171.56	5.95 \times	0.41 (-67.2%)	33.38 (-6.2%)	28.38	0.57	0.60
TaylorSeer($N=9$)\dagger	24.64 (-80.7%)	5.17 \times	2067.29	6.25 \times	0.73 (-41.6%)	32.97 (-7.4%)	28.25	0.56	0.58
FreqCa($N=10$)	22.45 (-82.4%)	5.68 \times	1809.38	7.14 \times	1.02 (-18.4%)	35.00 (-1.7%)	28.86	0.64	0.44
Qwen-Image-Lightning: 8 steps	7.27 (+0.0%)	1.00 \times	560.96	1.00 \times	1.30 (+0.0%)	35.26 (+0.0%)	∞	1.00	0.00
FreqCa($N=2$): 8 steps	5.29 (-27.2%)	1.37 \times	350.61	1.60 \times	1.29 (-0.8%)	35.23 (-0.1%)	33.01	0.83	0.12
FreqCa($N=3$): 8 steps	4.63 (-36.3%)	1.57 \times	282.26	1.99 \times	1.28 (-1.5%)	35.10 (-0.5%)	31.36	0.77	0.18
FreqCa($N=4$): 8 steps	3.29 (-54.9%)	2.21 \times	140.25	4.00 \times	1.29 (-0.8%)	35.94 (+1.9%)	29.25	0.62	0.36

• \dagger Methods exhibit significant degradation in image quality.

• Gray: Baseline-relative degradation in quality and gains in latency. Blue: **FreqCa** achieves minimal degradation with large latency gains.

4.3 IMAGE EDITING

4.3.1 FLUX.1-KONTEXT-DEV

On FLUX.1-Kontext-dev, *FreqCa* outperforms other acceleration methods. At **5.00 \times** speedup, *FreqCa* achieves a Q_O score of **6.195**, outperforming ToCa (6.125). At **6.24 \times** speedup, *FreqCa* shows only a **0.4%** drop in Q_O score, demonstrating better perceptual fidelity.

Table 3: **Quantitative comparison of text-to-image generation** for FLUX.1-Kontext-dev. Best results are highlighted in **bold**, and second-best are underlined.

Method	Acceleration				GEdit-EN (Full)		
	Latency(s) \downarrow	Speed \uparrow	FLOPs(T) \downarrow	Speed \uparrow	Q_SC \uparrow	Q_PQ \uparrow	Q_O \uparrow
[Kontext]50 steps	50.20 (+0.0%)	1.00 \times	8299.54	1.00 \times	6.481	7.331	6.213 (+0.0%)
50% steps \dagger	25.42 (-49.4%)	1.97 \times	4149.77	2.00 \times	6.544	7.286	6.253 (+0.6%)
20% steps \dagger	10.47 (-79.1%)	4.79 \times	1659.91	5.00 \times	6.603	7.184	6.286 (+1.2%)
ToCa($N=8, R=70\%$)	29.56 (-41.1%)	1.70 \times	1841.35	4.51 \times	6.432	7.256	6.125 (-1.4%)
DuCa($N=8, R=60\%$)	13.12 (-73.9%)	3.83 \times	1669.08	4.97 \times	6.469	7.195	6.150 (-1.0%)
TaylorSeer($N=6, O=2$)	<u>13.95</u> (-72.2%)	3.60 \times	1660.95	5.00 \times	6.477	7.296	6.170 (-0.7%)
FreqCa($N=7$)	10.77 (-78.5%)	4.66 \times	1661.37	5.00 \times	6.480	7.271	6.195 (-0.3%)
ToCa($N=12, R=75\%$)	20.72 (-58.7%)	2.42 \times	1359.61	6.10 \times	6.393	6.919	6.041 (-2.8%)
DuCa($N=12, R=70\%$)	10.39 (-79.3%)	4.83 \times	1376.55	6.03 \times	6.597	7.005	6.173 (-0.6%)
TaylorSeer($N=9, O=2$)	<u>12.05</u> (-76.0%)	4.17 \times	1329.02	6.24 \times	6.407	6.995	6.074 (-2.2%)
FreqCa($N=10$)	8.74 (-82.6%)	5.74 \times	1329.33	6.24 \times	6.550	7.160	6.190 (-0.4%)

• \dagger Methods exhibit significant degradation in image quality; Q_SC: semantic consistency, Q_PQ: perceptual quality, Q_O: overall score.

• Gray: Baseline-relative degradation in quality and gains in latency. Blue: **FreqCa** achieves minimal degradation with large latency gains.

4.3.2 QWEN-IMAGE-EDIT

Table 4: **Quantitative comparison of image editing** using Qwen-Image-Edit. Best results are highlighted in **bold**, and second-best are underlined.

Method	Acceleration				GEdit-CN (Full)			GEdit-EN (Full)		
	Latency(s) \downarrow	Speed \uparrow	FLOPs(T) \downarrow	Speed \uparrow	Q_SC \uparrow	Q_PQ \uparrow	Q_O \uparrow	Q_SC \uparrow	Q_PQ \uparrow	Q_O \uparrow
[full]50 steps	284.51 (+0.0%)	1.00 \times	28190.88	1.00 \times	7.68	7.51	7.41 (+0.0%)	7.82	7.54	7.54 (+0.0%)
50% steps \dagger	143.29 (-49.6%)	1.99 \times	14095.44	2.00 \times	7.70	7.53	7.44 (+0.4%)	7.77	7.52	7.47 (-0.9%)
20% steps \dagger	58.45 (-79.5%)	4.87 \times	5638.18	5.00 \times	7.65	7.42	7.35 (-0.8%)	7.73	7.46	7.44 (-1.3%)
FORA($N=5$)	<u>63.15</u> (-77.8%)	4.51 \times	5643.13	<u>5.00</u> \times	7.60	7.31	7.25 (-2.2%)	7.62	7.34	7.28 (-3.4%)
DuCa($N=7, R=95\%$)	69.54 (-75.5%)	4.09 \times	5699.89	4.95 \times	<u>7.73</u>	7.44	7.44 (+0.4%)	7.80	7.40	7.45 (-1.2%)
TaylorSeer($N=6, O=2$)	65.66 (-76.9%)	4.33 \times	5643.13	5.00 \times	7.25	7.09	6.92 (-6.6%)	7.26	7.14	6.89 (-8.6%)
FreqCa($N=6$)	62.89 (-77.9%)	4.52 \times	5642.24	5.00 \times	7.75	7.54	7.49 (+1.1%)	7.83	7.48	7.52 (-0.3%)
FORA($N=7$)	<u>52.20</u> (-81.7%)	<u>5.45</u> \times	<u>4515.74</u>	6.24 \times	7.42	7.13	7.06 (-4.7%)	7.43	7.19	7.06 (-6.3%)
DuCa($N=10, R=95\%$)	59.81 (-79.0%)	4.76 \times	5158.45	5.46 \times	<u>7.50</u>	5.75	6.39 (-13.8%)	<u>7.52</u>	5.77	6.41 (-15.0%)
TaylorSeer($N=9, O=2$)	53.92 (-81.1%)	5.28 \times	<u>4515.74</u>	6.24 \times	6.61	6.65	6.31 (-14.8%)	6.67	6.63	6.31 (-16.3%)
FreqCa($N=9$)	51.09 (-82.0%)	5.57 \times	4514.48	6.24 \times	7.62	7.18	7.27 (+1.9%)	7.66	7.12	7.21 (-4.3%)

• \dagger Methods exhibit significant degradation in image quality; Q_SC: semantic consistency, Q_PQ: perceptual quality, Q_O: overall score.

• Gray: Baseline-relative degradation in quality and gains in latency. Blue: **FreqCa** achieves minimal degradation with large latency gains.

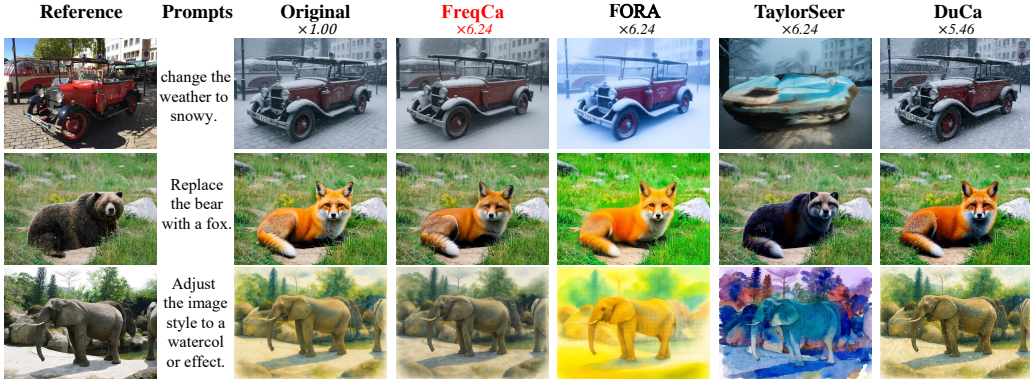


Figure 6: On Qwen-Image-Edit, *FreqCa* delivers higher speedup with near-original editing quality

On Qwen-Image-Edit, *FreqCa* demonstrates superior performance in bilingual editing tasks. At **5.00**× speedup, *FreqCa* achieves Q-O scores of 7.49 on GEdit-CN and 7.52 on GEdit-EN, outperforming TaylorSeer (6.92 and 6.89). At **6.24**× speedup, *FreqCa* shows quality drops of only **1.9%** and **4.3%**, while TaylorSeer degrades by 14.8% and 16.3%.

As shown in **Figures 5 and 6**, qualitative evaluation confirms *FreqCa*’s superior visual quality preservation. While FORA (6.24×), Duca(5.46×) and TaylorSeer (6.24×) exhibit significant artifacts, *FreqCa* (6.24×) maintains consistent visual quality comparable to the original model.

4.4 ABLATION STUDIES

4.4.1 CACHE MEMORY AND COMPUTATIONAL EFFICIENCY

Conventional layer-wise caching methods store both attention and MLP outputs per layer ($N = 2$) and retain $m + 1$ historical states for m -th order prediction, yielding memory cost $\mathcal{K}_{\text{layer}} = 2(m + 1)L$. For FLUX.1-dev ($L = 57$) with second-order prediction ($m = 2$), this requires 342 cache units.

In contrast, *FreqCa* caches only the CRF, adopting a frequency-decoupled strategy: low-frequency components are reused (1 unit), while high-frequency components employ second-order Hermite interpolation (3 units). The total cost is constant:

$$\mathcal{K}_{\text{FreqCa}} = 1 + 3 = 4, \quad R = \frac{\mathcal{K}_{\text{FreqCa}}}{\mathcal{K}_{\text{layer}}} = \frac{4}{(m + 1) \cdot N \cdot L} \approx 1.17\% \quad (m = 2, L = 57, N = 2),$$

reducing memory complexity from $\mathcal{O}(L)$ to $\mathcal{O}(1)$. Computationally, prediction steps incur negligible cost $C_{\text{pred}} \ll C_{\text{full}}$. Executing a full forward pass every S steps yields average cost:

$$\bar{C} = \frac{1}{S} C_{\text{full}} + (1 - \frac{1}{S}) C_{\text{pred}} \quad \Rightarrow \quad \text{Speedup} \approx S \quad \text{as } C_{\text{pred}} \rightarrow 0.$$

FreqCa achieves near-S× acceleration with only **1%** additional memory overhead, establishing the first constant-memory, high-throughput inference acceleration framework for diffusion models.

Table 5: **Comparison of methods in Cache Memory, MACs, Latency, and FLOPS on FLUX-1.dev**, Best results are highlighted in **bold**, and second-best results are underlined.

Method	VRAM Overhead (GB)↓	MACs (T)↓	Latency (s)↓	FLOPs (T)↓	Image Reward ↑
[dev]: 50 steps	0.62	1859.62	23.24	3726.87	0.99 (+0.0%)
ToCa ($\mathcal{N}=8, \mathcal{R}=75\%$)	12.31 (+11.69GB)	414.88	12.39	829.86	0.95 (-4.0%)
DuCa ($\mathcal{N}=8, \mathcal{R}=70\%$)	<u>3.65</u> (+3.63GB)	428.86	9.40	858.27	0.94 (-5.1%)
TeaCache ($l=1.0$)	<u>0.69</u> (+0.07GB)	409.43	7.07	820.55	0.84 (-15.2%)
TaylorSeer ($\mathcal{N}=6, O=2$)	7.66 (+7.02GB)	<u>372.38</u>	<u>6.73</u>	<u>746.28</u>	<u>1.00</u> (+1.0%)
FreqCa ($\mathcal{N}=7$)	0.69 (+0.07GB)	372.25	5.19	746.03	1.01 (+2.0%)

- **Note:** All methods inherit baseline memory optimizations (e.g., FlashAttention). ToCa is incompatible with these, hence its higher reported cache usage. **Actual cache memory usage** for each method should be computed as: VRAM Overhead – 0.62 GB.

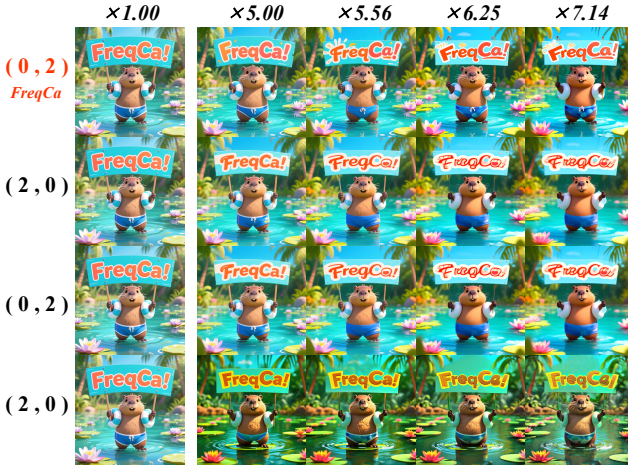


Figure 7: QwenImage ablation results showing image quality under different frequency prediction configurations and acceleration ratios. $(x, y) = (\text{low}, \text{high})$ prediction orders.

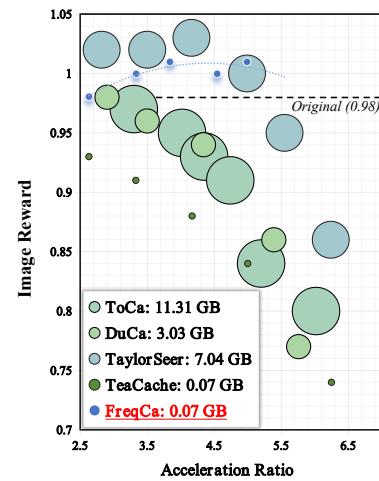


Figure 8: Imagereward versus speedup ratio across methods. Bubble size indicates cache memory.

4.4.2 DECOMPOSITION AND ORDER OF PREDICTION ABLATION STUDY

We perform an ablation study on FLUX.1-dev to identify the optimal frequency decomposition method and prediction order. The study compares three decomposition strategies including FFT, DCT, and a baseline without decomposition, each paired with various prediction approaches for frequency components. Figure 10 compares these optimized configurations. The results indicate that the DCT-based approach, particularly with low-frequency reuse and high-frequency prediction, achieves consistently high ImageReward across acceleration ratios and demonstrates marked superiority at larger intervals ($N > 8$). This robustness under high acceleration factors confirms the rationale for our choice. A separate ablation on Qwen-Image revealed that the FFT-based method with the same prediction strategy performed best. As shown in Figure 7, other configurations result in significant quality degradation when compared to our optimal settings.

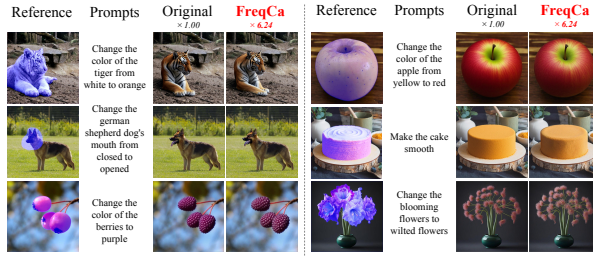


Figure 9: On FLUX.1-Fill-dev, *FreqCa* achieves 6.24 \times acceleration while preserving image inpainting quality indistinguishable from the original.

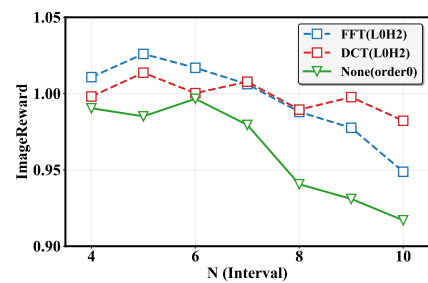


Figure 10: Comparing optimal predictors under varied frequency decompositions on FLUX across speedup ratios.

5 CONCLUSION

In this work, we presented *FreqCa*, a frequency-aware feature caching framework that unifies the strengths of reuse- and forecast-based paradigms. By decomposing features into low- and high-frequency components, *FreqCa* selectively reuses stable low-frequency features and accurately predicts dynamic high-frequency components, leading to a superior trade-off between acceleration and generation quality. Furthermore, by introducing Cumulative Residual Feature caching, we reduced the memory footprint to $\mathcal{O}(1)$, making frequency-aware caching practical even on consumer hardware. Extensive experiments across diverse diffusion models demonstrate that *FreqCa* achieves 6–7 \times acceleration with negligible quality degradation, establishing a new SOTA in efficient diffusion inference. We believe *FreqCa* opens up new possibilities for scalable, high-performance generative modeling and offers a general method for future research in frequency-aware acceleration techniques.

ETHICS STATEMENT

This work presents FreqCa, a technical method for accelerating diffusion model inference through frequency-aware caching. Our research focuses purely on computational efficiency improvements and does not introduce new ethical risks beyond those inherent to the underlying diffusion models. We use only publicly available models and datasets in our experiments, and our acceleration technique is model-agnostic and content-neutral. While our method reduces inference time and computational costs, which could potentially make generative AI more accessible, we acknowledge that this accessibility applies to both beneficial and potentially harmful use cases. We encourage responsible deployment of accelerated diffusion models in accordance with existing ethical guidelines for AI-generated content, including proper disclosure of synthetic media and consideration of potential societal impacts.

REPRODUCIBILITY STATEMENT

We are committed to ensuring the full reproducibility of our FreqCa framework. To this end, Section 3 provides the complete mathematical formulations for our core algorithmic components: frequency decomposition (FFT/DCT), Cumulative Residual Feature (CRF) caching, and second-order Hermite prediction. All experimental configurations are detailed in Section 4.1, specifying the models evaluated (e.g., FLUX.1-dev, Qwen-Image), the datasets used (DrawBench and GEdit), and the full set of evaluation metrics (e.g., ImageReward, CLIP Score, PSNR). Section 4 and the Appendix present our detailed ablation studies, hyperparameter choices for decomposition methods and prediction strategies, and the computational complexity analysis. An anonymous source code repository is provided in the supplementary materials, containing complete inference and training scripts, configuration files with random seeds, and data preprocessing pipelines. The repository will be made publicly available upon acceptance.

REFERENCES

Andreas Blattmann, Tim Dockhorn, Sumith Kulal, Daniel Mendelevitch, Maciej Kilian, Dominik Lorenz, Yam Levi, Zion English, Vikram Voleti, Adam Letts, et al. Stable video diffusion: Scaling latent video diffusion models to large datasets. *arXiv preprint arXiv:2311.15127*, 2023.

Daniel Bolya and Judy Hoffman. Token merging for fast stable diffusion. In *Proceedings of the IEEE/CVF conference on computer vision and pattern recognition*, pp. 4599–4603, 2023.

Pengtao Chen, Mingzhu Shen, Peng Ye, Jianjian Cao, Chongjun Tu, Christos-Savvas Bouganis, Yiren Zhao, and Tao Chen. δ -dit: A training-free acceleration method tailored for diffusion transformers. *arXiv preprint arXiv:2406.01125*, 2024.

Zhiyuan Chen, Keyi Li, Yifan Jia, Le Ye, and Yufei Ma. Accelerating diffusion transformer via increment-calibrated caching with channel-aware singular value decomposition, 2025.

Huanpeng Chu, Wei Wu, Guanyu Fen, and Yutao Zhang. Omnicache: A trajectory-oriented global perspective on training-free cache reuse for diffusion transformer models, 2025.

Gongfan Fang, Xinyin Ma, and Xinchao Wang. Structural pruning for diffusion models. *arXiv preprint arXiv:2305.10924*, 2023.

Liang Feng, Shikang Zheng, Jiacheng Liu, Yuqi Lin, Qinming Zhou, Peiliang Cai, Xinyu Wang, Junjie Chen, Chang Zou, Yue Ma, and Linfeng Zhang. Hicache: Training-free acceleration of diffusion models via hermite polynomial-based feature caching, 2025.

Jack Hessel, Ari Holtzman, Maxwell Forbes, Ronan Le Bras, and Yejin Choi. Clipscore: A reference-free evaluation metric for image captioning. *arXiv preprint arXiv:2104.08718*, 2021.

Jonathan Ho, Ajay Jain, and Pieter Abbeel. Denoising Diffusion Probabilistic Models, December 2020a. URL <http://arxiv.org/abs/2006.11239>. arXiv:2006.11239 [cs].

Jonathan Ho, Ajay Jain, and Pieter Abbeel. Denoising diffusion probabilistic models. *Advances in neural information processing systems*, 33:6840–6851, 2020b.

Minchul Kim, Shangqian Gao, Yen-Chang Hsu, Yilin Shen, and Hongxia Jin. Token fusion: Bridging the gap between token pruning and token merging. In *Proceedings of the IEEE/CVF Winter Conference on Applications of Computer Vision*, pp. 1383–1392, 2024.

Sungbin Kim, Hyunwuk Lee, Wonho Cho, Mincheol Park, and Won Woo Ro. Ditto: Accelerating diffusion model via temporal value similarity. In *Proceedings of the 2025 IEEE International Symposium on High-Performance Computer Architecture (HPCA)*. IEEE, 2025.

Black Forest Labs. Flux. <https://github.com/black-forest-labs/flux>, 2024.

Senmao Li, Taihang Hu, Fahad Shahbaz Khan, Linxuan Li, Shiqi Yang, Yaxing Wang, Ming-Ming Cheng, and Jian Yang. Faster diffusion: Rethinking the role of unet encoder in diffusion models. *arXiv preprint arXiv:2312.09608*, 2023a.

Xiuyu Li, Yijiang Liu, Long Lian, Huanrui Yang, Zhen Dong, Daniel Kang, Shanghang Zhang, and Kurt Keutzer. Q-diffusion: Quantizing diffusion models. In *2023 IEEE/CVF International Conference on Computer Vision (ICCV)*, pp. 17489–17499, 2023b. doi: 10.1109/ICCV51070.2023.01608.

Yanyu Li, Huan Wang, Qing Jin, Ju Hu, Pavlo Chemerys, Yun Fu, Yanzhi Wang, Sergey Tulyakov, and Jian Ren. Snapfusion: Text-to-image diffusion model on mobile devices within two seconds. *Advances in Neural Information Processing Systems*, 36, 2024.

Jiacheng Liu, Chang Zou, Yuanhuiyi Lyu, Junjie Chen, and Linfeng Zhang. From reusing to forecasting: Accelerating diffusion models with taylorseers, 2025a.

Jiacheng Liu, Chang Zou, Yuanhuiyi Lyu, Kaixin Li, Shaobo Wang, and Linfeng Zhang. Specia: Accelerating diffusion transformers with speculative feature caching. In *Proceedings of the 33rd ACM International Conference on Multimedia (MM '25)*, pp. to appear, Dublin, Ireland, October 2025b. ACM.

Xingchao Liu, Chengyue Gong, and Qiang Liu. Rectified flow: A general and versatile method for generative modeling, 2023a. URL <https://arxiv.org/abs/2210.11493>.

Xingchao Liu, Chengyue Gong, et al. Flow straight and fast: Learning to generate and transfer data with rectified flow. In *The Eleventh International Conference on Learning Representations*, 2023b.

Ziming Liu, Yifan Yang, Chengruidong Zhang, Yiqi Zhang, Lili Qiu, Yang You, and Yuqing Yang. Region-adaptive sampling for diffusion transformers, 2025c. URL <https://arxiv.org/abs/2502.10389>.

Cheng Lu, Yuhao Zhou, Fan Bao, Jianfei Chen, Chongxuan Li, and Jun Zhu. Dpm-solver: A fast ode solver for diffusion probabilistic model sampling in around 10 steps. *Advances in Neural Information Processing Systems*, 35:5775–5787, 2022a.

Cheng Lu, Yuhao Zhou, Fan Bao, Jianfei Chen, Chongxuan Li, and Jun Zhu. Dpm-solver++: Fast solver for guided sampling of diffusion probabilistic models. *arXiv preprint arXiv:2211.01095*, 2022b.

Zhengyao Lv, Chenyang Si, Junhao Song, Zhenyu Yang, Yu Qiao, Ziwei Liu, and Kwan-Yee K. Wong. FasterCache: Training-Free Video Diffusion Model Acceleration with High Quality, 2025.

Xinyin Ma, Gongfan Fang, and Xinchao Wang. Deepcache: Accelerating diffusion models for free. In *Proceedings of the IEEE/CVF Conference on Computer Vision and Pattern Recognition*, pp. 15762–15772, 2024.

Chenlin Meng, Ruiqi Gao, Diederik P Kingma, Stefano Ermon, Jonathan Ho, and Tim Salimans. On distillation of guided diffusion models. In *NeurIPS 2022 Workshop on Score-Based Methods*, 2022. URL <https://openreview.net/forum?id=6QHpsQt6VR->.

William Peebles and Saining Xie. Scalable Diffusion Models with Transformers, March 2023a. URL <http://arxiv.org/abs/2212.09748>. arXiv:2212.09748 [cs].

William Peebles and Saining Xie. Scalable diffusion models with transformers. In *Proceedings of the IEEE/CVF International Conference on Computer Vision*, pp. 4195–4205, 2023b.

Junxiang Qiu, Shuo Wang, Jinda Lu, Lin Liu, Houcheng Jiang, and Yanbin Hao. Accelerating diffusion transformer via error-optimized cache, 2025. URL <https://arxiv.org/abs/2501.19243>.

Robin Rombach, Andreas Blattmann, Dominik Lorenz, Patrick Esser, and Björn Ommer. High-Resolution Image Synthesis with Latent Diffusion Models, April 2022. URL <http://arxiv.org/abs/2112.10752> [cs]. arXiv:2112.10752 [cs].

Olaf Ronneberger, Philipp Fischer, and Thomas Brox. U-net: Convolutional networks for biomedical image segmentation. In *Medical image computing and computer-assisted intervention—MICCAI 2015: 18th international conference, Munich, Germany, October 5–9, 2015, proceedings, part III* 18, pp. 234–241. Springer, 2015.

Chitwan Saharia, William Chan, Saurabh Saxena, Lala Li, Jay Whang, Emily Denton, Seyed Kamyar Seyed Ghasemipour, Burcu Karagol Ayan, S. Sara Mahdavi, Rapha Gontijo Lopes, Tim Salimans, Jonathan Ho, David J. Fleet, and Mohammad Norouzi. Photorealistic text-to-image diffusion models with deep language understanding. In *Proceedings of the IEEE/CVF Conference on Computer Vision and Pattern Recognition*, pp. 24219–24238, 2022.

Tim Salimans and Jonathan Ho. Progressive distillation for fast sampling of diffusion models. *arXiv preprint arXiv:2202.00512*, 2022.

Pratheba Selvaraju, Tianyu Ding, Tianyi Chen, Ilya Zharkov, and Luming Liang. Fora: Fast-forward caching in diffusion transformer acceleration. *arXiv preprint arXiv:2407.01425*, 2024.

Yuzhang Shang, Zhihang Yuan, Bin Xie, Bingzhe Wu, and Yan Yan. Post-training quantization on diffusion models. In *Proceedings of the IEEE/CVF conference on computer vision and pattern recognition*, pp. 1972–1981, 2023.

Jascha Sohl-Dickstein, Eric Weiss, Niru Maheswaranathan, and Surya Ganguli. Deep unsupervised learning using nonequilibrium thermodynamics. In *International conference on machine learning*, pp. 2256–2265. PMLR, 2015.

Jiaming Song, Chenlin Meng, and Stefano Ermon. Denoising diffusion implicit models. In *International Conference on Learning Representations*, 2021.

Yang Song, Prafulla Dhariwal, Mark Chen, and Ilya Sutskever. Consistency models. In *International Conference on Machine Learning*, pp. 32211–32252. PMLR, 2023.

Andreas Veit, Michael J Wilber, and Serge Belongie. Residual networks behave like ensembles of relatively shallow networks. *Advances in neural information processing systems*, 29, 2016.

Wen Wang, Qifeng Chen, Lvmin Zhang, Yue Ma, and Zexuan Yan. Gedit: A unified metric for evaluating instruction-based image editing. In *Proceedings of the IEEE/CVF Conference on Computer Vision and Pattern Recognition*, pp. 12345–12354, 2024.

Zhou Wang, A.C. Bovik, H.R. Sheikh, and E.P. Simoncelli. Image quality assessment: From error visibility to structural similarity. *IEEE Transactions on Image Processing*, 13(4):600–612, 2004. doi: 10.1109/TIP.2003.819861.

Jiazheng Xu, Xiao Liu, Yuchen Wu, Yuxuan Tong, Qinkai Li, Ming Ding, Jie Tang, and Yuxiao Dong. Imagereward: Learning and evaluating human preferences for text-to-image generation, 2023. URL <https://arxiv.org/abs/2304.05977>.

Zhuoyi Yang, Jiayan Teng, Wendi Zheng, Ming Ding, Shiyu Huang, Jiazheng Xu, Yuanming Yang, Wenyi Hong, Xiaohan Zhang, Guanyu Feng, Da Yin, Xiaotao Gu, Yuxuan Zhang, Weihan Wang, Yean Cheng, Bin Xu, Yuxiao Dong, and Jie Tang. Cogvideox: Text-to-video diffusion models with an expert transformer. In *The Thirteenth International Conference on Learning Representations*, 2025. URL <https://openreview.net/forum?id=LQzN6TRFg9>.

Evelyn Zhang, Bang Xiao, Jiayi Tang, Qianli Ma, Chang Zou, Xuefei Ning, Xuming Hu, and Linfeng Zhang. Token pruning for caching better: 9 times acceleration on stable diffusion for free, 2024. URL <https://arxiv.org/abs/2501.00375>.

Evelyn Zhang, Jiayi Tang, Xuefei Ning, and Linfeng Zhang. Training-free and hardware-friendly acceleration for diffusion models via similarity-based token pruning. In *Proceedings of the AAAI Conference on Artificial Intelligence*, 2025.

Lvmi Zhang and Maneesh Agrawala. Flux.1 kontext: Flow matching for in-context image generation and editing, 2025. URL <https://arxiv.org/abs/2506.15742>.

Richard Zhang, Phillip Isola, Alexei A. Efros, Eli Shechtman, and Oliver Wang. The Unreasonable Effectiveness of Deep Features as a Perceptual Metric, 2018.

Xuanlei Zhao, Xiaolong Jin, Kai Wang, and Yang You. Real-time video generation with pyramid attention broadcast. *arXiv preprint arXiv:2408.12588*, 2024.

Kaiwen Zheng, Cheng Lu, Jianfei Chen, and Jun Zhu. DPM-solver-v3: Improved diffusion ODE solver with empirical model statistics. In *Thirty-seventh Conference on Neural Information Processing Systems*, 2023. URL <https://openreview.net/forum?id=9fWKExmKa0>.

Shikang Zheng, Liang Feng, Xinyu Wang, Qinming Zhou, Peiliang Cai, Chang Zou, Jiacheng Liu, Yuqi Lin, Junjie Chen, Yue Ma, and Linfeng Zhang. Forecast then calibrate: Feature caching as ode for efficient diffusion transformers, 2025.

Zangwei Zheng, Xiangyu Peng, Tianji Yang, Chenhui Shen, Shenggui Li, Hongxin Liu, Yukun Zhou, Tianyi Li, and Yang You. Open-sora: Democratizing efficient video production for all, March 2024. URL <https://github.com/hpcaitech/Open-Sora>.

Haowei Zhu, Dehua Tang, Ji Liu, Mingjie Lu, Jintu Zheng, Jinzhang Peng, Dong Li, Yu Wang, Fan Jiang, Lu Tian, Spandan Tiwari, Ashish Sirasao, Jun-Hai Yong, Bin Wang, and Emad Barsoum. Dip-go: A diffusion pruner via few-step gradient optimization, 2024.

Chang Zou, Evelyn Zhang, Runlin Guo, Haohang Xu, Conghui He, Xuming Hu, and Linfeng Zhang. Accelerating diffusion transformers with dual feature caching, 2024. URL <https://arxiv.org/abs/2412.18911>.

Chang Zou, Xuyang Liu, Ting Liu, Siteng Huang, and Linfeng Zhang. Accelerating diffusion transformers with token-wise feature caching. In *Proceedings of the 13th International Conference on Learning Representations (ICLR 2025)*. ICLR, 2025. URL <https://openreview.net/forum?id=yYZbZGo4ei>. accepted to ICLR 2025.

APPENDIX

A USE OF LARGE LANGUAGE MODELS

No Large Language Models were used in this research. All research ideas, algorithmic designs, experimental methodologies, data analysis, and manuscript writing were entirely completed by the authors independently.

B DETAILED EXPERIMENTAL SETUP

This section provides comprehensive technical details for all experimental configurations mentioned in Section 4.1.

B.1 MODEL AND TASK SPECIFICATIONS

FLUX.1-dev and Qwen-Image: The images generated by the FLUX.1-dev, FLUX.1-schnell, and Qwen-Image-Lightning models are obtained at 1024x1024 resolution using 200 high-quality prompts sourced from the DrawBench benchmark, while those generated by Qwen-Image were obtained at 1328×1328 resolutions. Quality assessment is performed using ImageReward, a robust perceptual metric for text-to-image alignment.

FLUX.1-Kontext-dev and Qwen-Image-Edit: We employ the FLUX.1-Kontext-dev and Qwen-Image-Edit model for image editing synthesis. Images editing and quality assessment is performed using GEdit benchmark, which grounded in real-world usages is developed to support more authentic and comprehensive evaluation of image editing models.

B.2 HARDWARE AND COMPUTATIONAL RESOURCES

All experiments are conducted on enterprise-grade GPU infrastructure:

- FLUX.1-dev experiments: NVIDIA A100 GPU
- FLUX.1-Kontext-dev experiments: NVIDIA A100 GPU
- Qwen-Image experiments: NVIDIA H20 GPU
- Qwen-Image-Edit experiments: NVIDIA H20 GPU

B.3 FREQCA IMPLEMENTATION PARAMETERS

- FLUX.1-dev experiments: DCT-based frequency decomposition was adopted.
- FLUX.1-Kontext-dev experiments: DCT-based frequency decomposition was adopted.
- Qwen-Image experiments: FFT-based frequency decomposition was adopted.
- Qwen-Image-Edit experiments: FFT-based frequency decomposition was adopted.

C DECOMPOSITION AND ORDER OF PREDICTION ABLATION STUDY

As shown in Figure C1, we systematically compared classical frequency decomposition methods (FFT and DCT) with a baseline that does not perform any frequency decomposition. The results clearly demonstrate that frequency decomposition plays a critical role in stabilizing model performance: omitting decomposition leads to a sharp drop in ImageReward scores, whereas both FFT and DCT significantly mitigate this degradation and maintain stable quality across timesteps. Furthermore, we investigated the impact of different prediction orders for low- and high-frequency components. We observe that inappropriate prediction strategies can easily introduce errors and harm generation quality. Among all tested configurations, the combination of zeroth-order prediction (direct reuse) for low-frequency components and second-order prediction for high-frequency components achieves consistently superior results, validating our hypothesis that low-frequency features should be reused directly while high-frequency components benefit from higher-order modeling. These findings

confirm the necessity of frequency-aware design and provide empirical guidance for selecting optimal prediction strategies.

C.1 PREDICTION ORDER COMBINATIONS

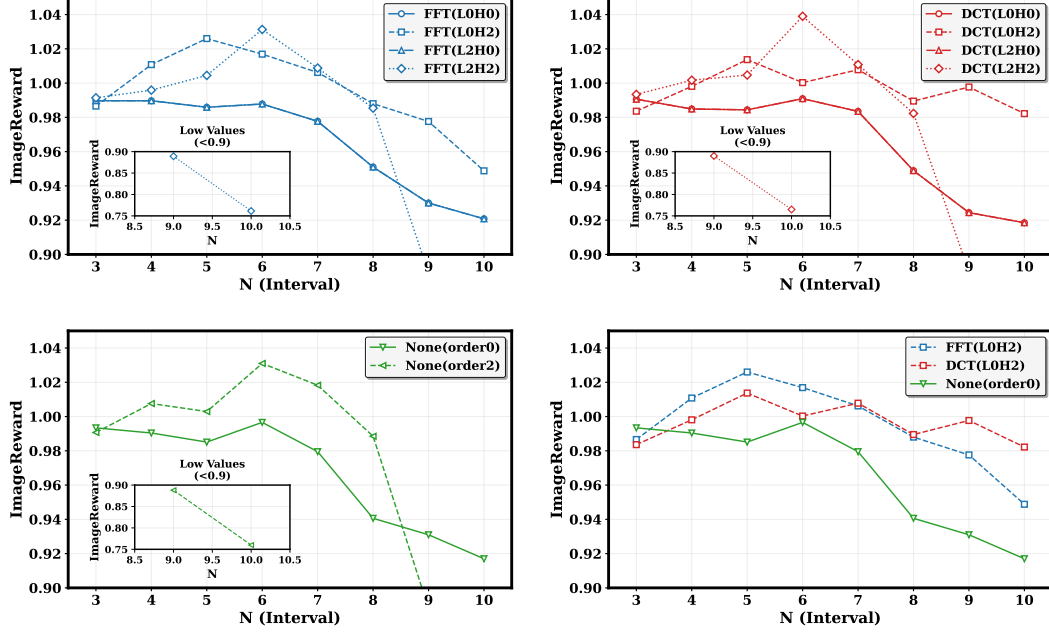


Figure C1: The ImageReward scores of FLUX.1-dev’s decomposition strategies (FFT, DCT, no-decomposition) paired with different frequency prediction approaches are presented here. This content includes the optimal prediction method for each decomposition strategy where low-frequency reuse and high-frequency prediction apply to FFT and DCT, and direct reuse applies to the no-decomposition (None) strategy.